Available online at www.sciencedirect.com
ScienceDirect
Ceramics International 36 (2010) 1495–1501
CERAMICS INTERNATIONAL
www.elsevier.com/locate/ceramint

Electrical behavior against current impulse in $ZnO–Pr_6O_{11}$-based varistor ceramics with terbium addition

Choon-W. Nahm *

Semiconductor Ceramics Lab., Department of Electrical Engineering, Dongeui University, Busan 614-714, Republic of Korea

Received 17 December 2009; received in revised form 6 January 2010; accepted 1 February 2010
Available online 9 March 2010

Abstract

Tb_4O_7 addition effect on electrical behavior against current impulse in the Zn–Pr–Co–Cr-based varistors was investigated. The Tb_4O_7 did have a significant effect on electrical behavior against current impulse. Increasing Tb_4O_7 content improved the clamp ratio (K), reaching nearly 2 at 1.0 mol%. The best stability against current impulse of 100 A/cm^2 was obtained at 0.25 mol% Tb_4O_7, where $\%\Delta E_{1\,mA/cm^2} = -0.8\%$ and $\%\Delta\alpha = +1.1\%$. In addition, the varistor doped with 0.5 mol% Tb_4O_7 were no less stable against current impulse than varistor doped with 0.25 mol% Tb_4O_7. Furthermore, the varistor doped with 0.5 mol% Tb exhibited the best surge withstand capability at a current impulse of 900 A. Conclusively, Tb_4O_7 content was optimized at 0.5 mol% in terms of the nonlinearity and surge withstand capability.

Keywords: Ceramics; Electrical properties; Current impulse; Varistors

1. Introduction

ZnO varistors are semiconducting electroceramic devices fabricated by sintering ZnO powders with minor additives, such as Bi_2O_3, Pr_6O_{11}, CoO, Cr_2O_3, etc [1,2]. Sintering process gives rise to a structure, which consists of semiconducting *n*-type ZnO grains surrounded by very thin insulating intergranular layers. Their nonlinear electrical characteristics are related to a unit structure composed of ZnO grain-intergranular layer-ZnO grain in the bulk of the devices. A unit structure acts as if it has a semiconductor junction at grain boundary. Since the nonlinear electrical behavior occurs at a boundary of each semiconducting ZnO grain, the varistor ceramics can be considered a multi-junction device composed of many series and parallel connection of grain boundary [3].

Transient voltages result from the sudden release of previously stored energy from overstress conditions such as lightning, inductive load switching, electromagnetic pulses or electrostatic discharges. Various electronic devices and electric power systems can be subjected to voltage transients (called surges) induced by lightning, switching, and electrostatic discharge. They are vulnerable to damage by surges in excess of their voltage ratings. Therefore, they should be protected from various surges.

The varistors have been extensively used in the field of circuit overvoltage protection, with application ranging from a few volts in electronic circuits to millions of volts in electric power systems [1,2].

Recently, $ZnO–Pr_6O_{11}$-based ceramics have been studied to further enhance the varistor properties and the stability against various stresses, compared with $ZnO–Bi_2O_3$-based varistor ceramics. Many investigations for $ZnO–Pr_6O_{11}$-based varistor ceramics have been reported on the microstructure and electrical properties in terms of additives, and sintering temperature and time [4–15]. In particular, the effect of rare earth oxides (Pr_6O_{11}, Er_2O_3, Dy_2O_3, Tb_4O_7, etc) on electrical properties and its stability [7–14]. But, a study on the stability of the varistor properties against current impulse with a high energy has been rarely reported.

In this work, the electrical behavior against current impulse in the Zn–Pr–Co–Cr (ZPCC)-based varistors was investigated with Tb_4O_7 content and some new results were obtained.

2. Experimental procedure

2.1. Sample preparation

Reagent-grade raw materials were used in proportions of $(98.0 - x)$ mol% ZnO, 0.5 mol% Pr_6O_{11}, 1.0 mol% CoO,

* Tel.: +82 51 890 1669; fax: +82 51 890 1664.
E-mail address: cwnahm@deu.ac.kr.

0272-8842/$36.00
doi:10.1016/j.ceramint.2010.02.027

0.5 mol% Cr_2O_3, x mol% Tb_4O_7 ($x = 0.0$, 0.25, 0.5, 0.75, 1.0). Raw materials were mixed by ball milling with zirconia balls and acetone in a polypropylene bottle for 24 h. The mixture was dried at 120 °C for 12 h and calcined in air at 750 °C for 2 h. The calcined mixture was pulverized using an agate mortar/pestle and after 2 wt% polyvinyl alcohol (PVA) binder addition, granulated by sieving through a 100-mesh screen to produce the starting power. The power was uniaxially pressed into discs of 10 mm in diameter and 2 mm in thickness at a pressure of 80 MPa. The discs were sintered at 1350 °C in air for 1 h and furnace-cooled to room temperature. The sintered samples were lapped and polished to 1.0 mm thickness. The final samples were about 8 mm in diameter and 1.0 mm in thickness. Silver paste was coated on both faces of samples and the silver electrodes were formed by heating it at 600 °C for 10 min. The electrodes were 5 mm in diameter.

2.2. Microstructure analysis

Both surfaces of the samples were lapped and ground with SiC paper and polished with 0.3 μm-Al_2O_3 powder to a mirror-like surface. The polished samples were thermally etched at 1100 °C for 30 min. The surface microstructure was examined by a scanning electron microscope (SEM, Hitachi S40, Japan). The average grain size (d) was determined by the lineal intercept method, given by $d = 1.56L/MN$, where L is the random line length on the micrograph, M is the magnification of the micrograph, and N is the number of the grain boundaries intercepted by the lines [16]. The sintered density (ρ) of ceramics was measured by the Archimedes method.

2.3. Electrical measurement

The electric field–current density (E–J) characteristics were measured using a V–I source (Keithley 237). The breakdown field ($E_{1\,mA/cm^2}$) was measured at 1.0 mA/cm^2 and the leakage current density (J_L) was measured at $0.8E_{1\,mA/cm^2}$. In addition, the nonlinear coefficient (α) is defined by the empirical law, $J = CE^{\alpha}$, where J is the current density, E is the applied electric field, and C is a constant. α was determined in the current density range of 1.0–10 mA/cm^2, where $\alpha = 1/(\log E_2 - \log E_1)$, and E_1 and E_2 are the electric fields corresponding to 1.0 mA/cm^2 and 10 mA/cm^2, respectively.

2.4. Clamping voltage measurement

The clamping voltage (V_c) was measured at a current impulse (I_p, 8 × 20 μs wave) of 5 A, 10 A, 25 A, and 50 A using a surge generator (Tae-yang Eng. Kor) and oscilloscope (TeK 3020B). The clamp ratio ($K = V_c/V_{1\,mA}$) is defined by ratio of clamping voltage to varistor voltage. The varistor voltage ($V_{1\,mA}$) was measured at a current of 1.0 mA DC.

2.5. Current impulse aging test

The current impulse aging test was performed under the following conditions with a current impulse (8 × 20 μs wave) of 100 A/cm^2 using a surge generator (Tae-yang Eng. Kor) and oscilloscope (TeK 3020B): (i) the number of 1st applied current impulse: 100 times, (ii) the number of 2nd applied current impulse: 400 times, (iii) the number of 3rd applied current impulse: 700 times, (iv) the number of 4th applied current impulse: 1000 times. The time interval between two current

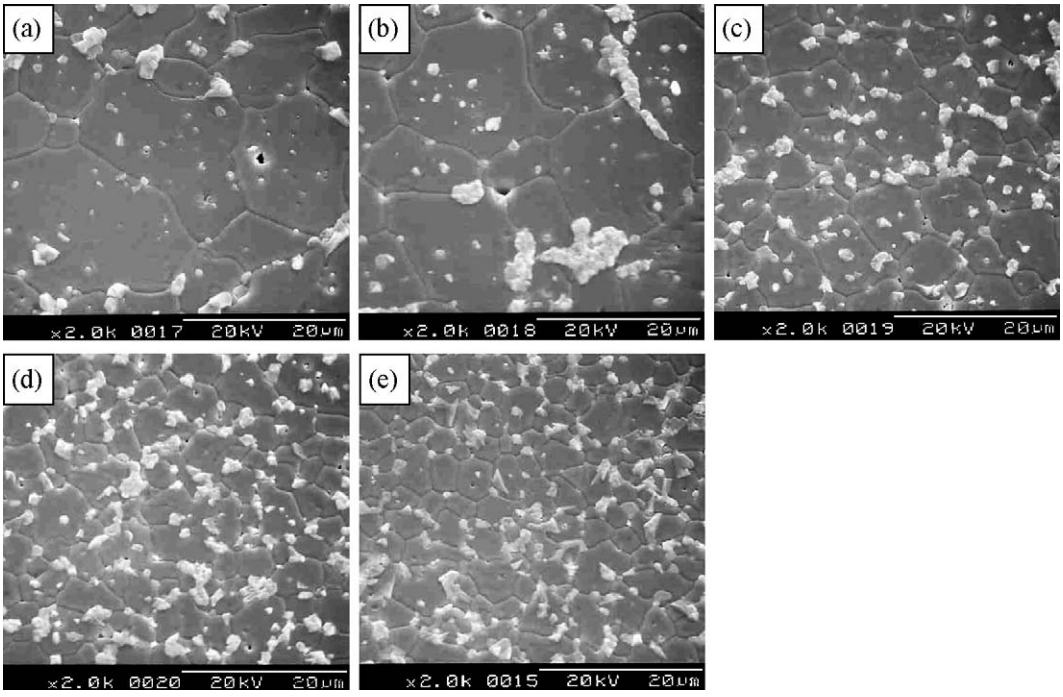

Fig. 1. SEM micrographs of the samples with different Tb_4O_7 contents : (a) 0.0 mol%, (b) 0.25 mol%, (c) 0.5 mol%, (d) 0.75 mol%, and (e) 1.0 mol%..

impulses was 2 s and the time interval between each current impulse cycles was 15 min. After applying the respective current impulse cycle, the *V–I* characteristics were measured at room temperature.

2.6. Surge withstand capability test

The surge withstand capability (SWC) test was performed at a current impulse (8 × 20 μs wave) of 500 A and 900 A using a surge generator (Tae-yang Eng. Kor) and oscilloscope (TeK 3020B). After applying the respective current impulse cycle, the *V–I* characteristics were measured at room temperature.

3. Results and discussion

Fig. 1 shows SEM micrographs of the samples for different Tb_4O_7 contents [14]. The microstructure consisted of primary phase ZnO grain, and Pr oxide and Tb_4O_7 as the secondary phases [14]. The majority of Tb_4O_7 and Pr oxide was segregated to grain boundaries and triple points due to the ionic radius difference for Zn. As Tb_4O_7 content increased, the secondary phases gradually increased through entire ceramics. The distribution of a secondary phase will have a significant effect on electrical properties against current impulse. The sintered density increased from 5.73 g/cm^3 to 5.85 g/cm^3 (5.78 g/cm^3 in pure ZnO) in accordance with increasing Tb_4O_7 content. There is nearly no porosity through the surface microstructure. The average grain size greatly decreased from 13.1 μm to 5.0 μm. This decrease is attributed to the restriction of grain growth by the increase of secondary phase in accordance with increasing Tb_4O_7 content.

Fig. 2 shows the *E–J* characteristics of the varistors doped for different Tb_4O_7 contents. It is well known that the conduction characteristics of the varistors are divided greatly into two regions: linear region (high impedance) before breakdown field and nonlinear region (low impedance) after breakdown field. The sharper knee of the curves between the two regions leads to the better nonlinear properties. As Tb_4O_7

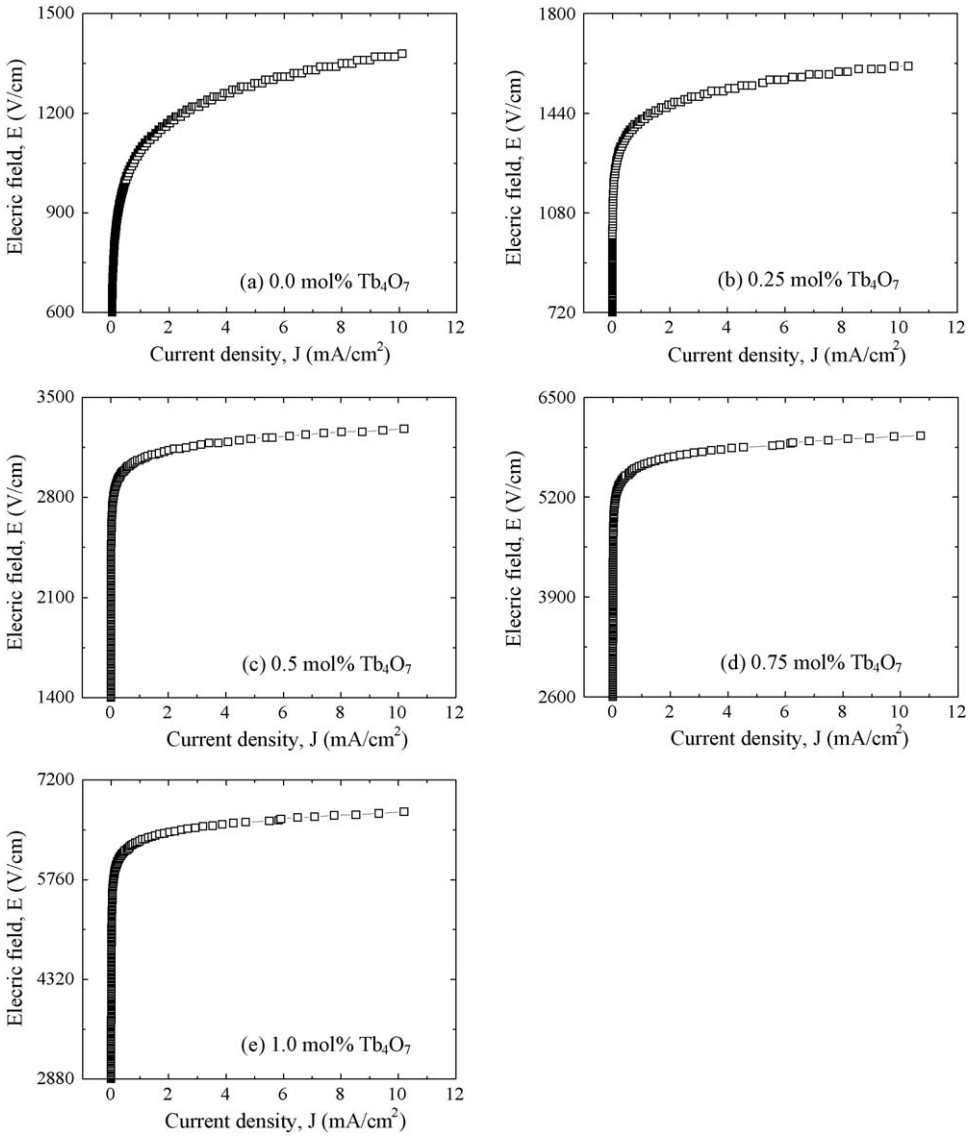

Fig. 2. *E–J* characteristics of the samples with different Tb_4O_7 contents.

Table 1
E–J characteristic parameters, clamping voltage, and clamping voltage ratio of the samples for different Tb_4O_7 contents.

T b_4O_7 content (mol%)	$E_{1\,mA/cm^2}$ (V/cm)	α	$V_{1\,mA}$ (V/mm)	V_c (V)				$K = V_c/V_{1\,mA}$			
				I_p = 5 A	10 A	25 A	50 A	I_p = 5 A	10 A	25 A	50 A
0.0	1087	9.8	129.1	316	344	348	432	2.45	2.66	2.69	3.34
0.25	1414	17.8	154.6	336	360	398	436	2.17	2.32	2.57	2.82
0.5	3064	34.3	321.2	570	608	666	714	1.77	1.89	2.07	2.22
0.75	5610	35.0	586.0	1070	1140	1210	1300	1.82	1.94	2.06	2.21
1.0	6322	37.2	660.6	1100	1180	1310	1420	1.66	1.78	1.98	2.15

content increased, the knee gradually became more pronounced and the nonlinear properties were enhanced. Therefore, the moderate Tb_4O_7 content seems to remarkably enhance the nonlinear properties. The detailed *E–J* parameters are summarized in Table 1. The breakdown field ($E_{1\,mA/cm^2}$) greatly increased from 1087 V/cm to 6322 V/cm in accordance with increasing Tb_4O_7 content. The $E_{1\,mA/cm^2}$ is proportional to the number of grain boundaries between the two electrodes. This indicates that the $E_{1\,mA/cm^2}$ is proportional to the inverse of the ZnO grain size: $E_{1\,mA/cm^2} = v_{gb}/d$, where v_{gb} is breakdown voltage and d is grain size. The increase of $E_{1\,mA/cm^2}$ in accordance with increasing Tb_4O_7 content can be explained by the increase in the number of grain boundaries owing to the decrease of average ZnO grain size, as mentioned in microstructure. The nonlinear coefficient (α) of the Tb_4O_7-undoped varistors was only 9.8, whereas the α value of the Tb_4O_7-doped varistors increased remarkably in the range of 17.8–37.2 in accordance with increasing Tb_4O_7 content. However, α is approximately saturated 35 at Tb_4O_7 content beyond 0.5 mol%. If the inherent role of varistor, that is, a surge withstand capability is low, even though the nonlinearity is good and the stability against DC accelerated aging stress is high, it is difficult to apply the varistors to the electrical and electronic fields. So, a surge withstand capability is no less important than others.

Figs. 3 and 4 show the clamping voltage (V_c) characteristics corresponding to various current impulses for the varistors doped with 0.25 mol% and 0.5 mol% Tb_4O_7, respectively. The V_c is defined by the drop voltage between electrodes of varistor when the specified current impulse flows through varistor. The higher current impulse leads to the higher V_c because the resistance in the nonlinear region exists still as a low value. It can be seen that the higher breakdown voltage leads to the higher clamping voltage. The detailed clamping voltage (V_c) and clamp ratio (K) against current impulse is summarized in Table 1. The low K value means that the varistor clamps a current impulse to operating voltage. The Tb_4O_7-undoped varistors exhibited the higher K value than Tb_4O_7-doped

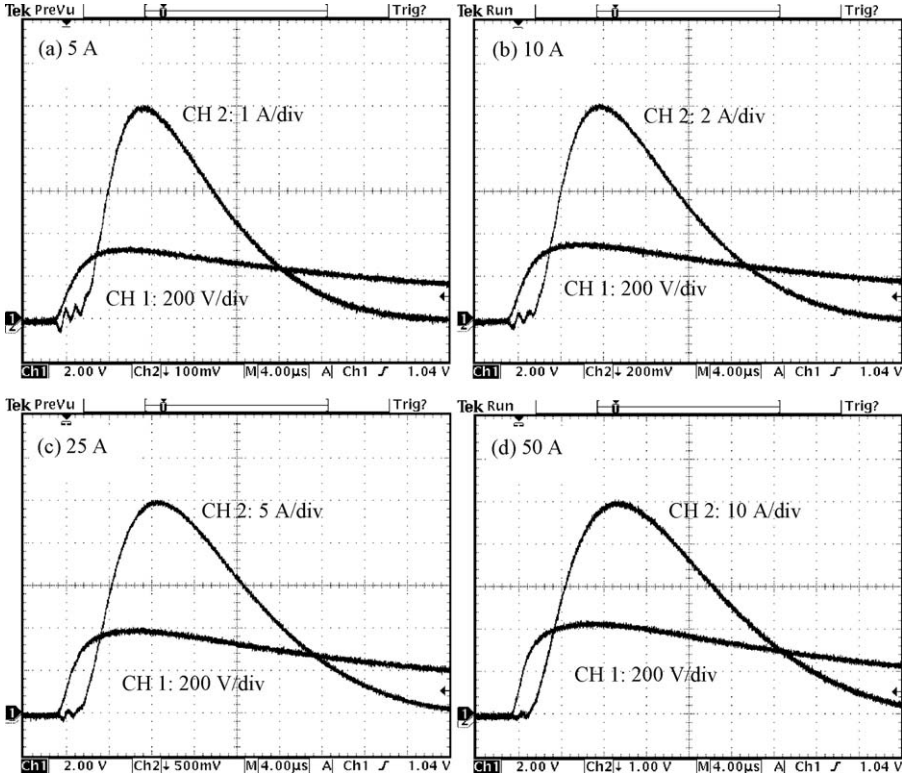

Fig. 3. Clamping voltage waveform for a current impulse of the varistor doped with 0.25 mol% Tb_4O_7.

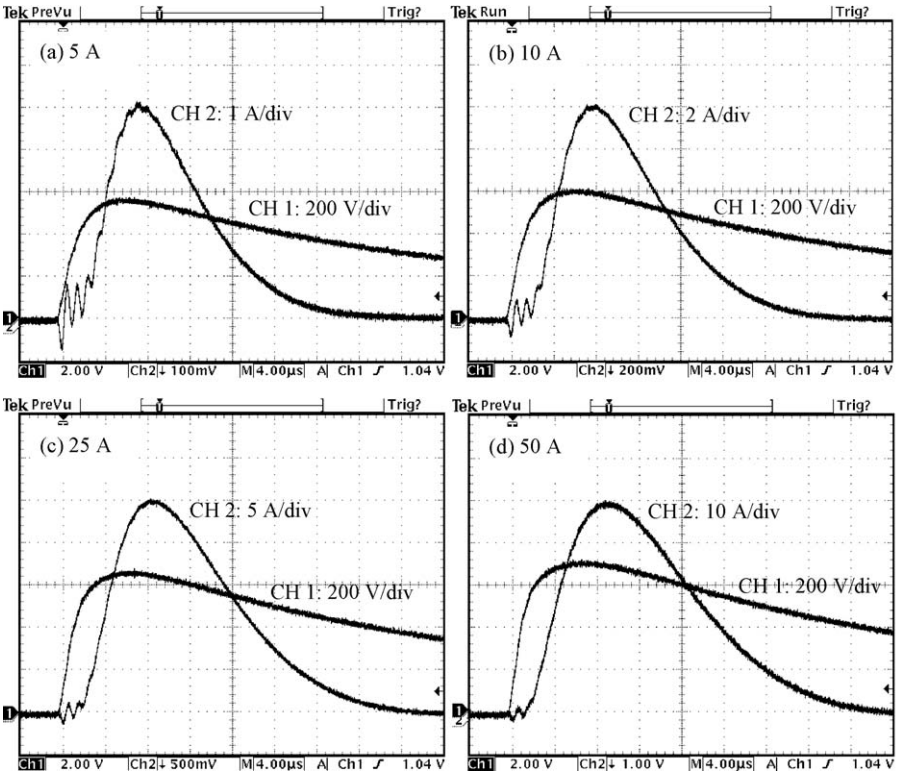

Fig. 4. Clamping voltage waveform for a current impulse of the varistor doped with 0.5 mol% Tb_4O_7.

varistors due to low nonlinear coefficient comparatively. Furthermore, the K value decreased with the increase of Tb_4O_7 content at arbitrary specified current impulse. The varistor doped with 1.0 mol% Tb_4O_7 exhibited inside and outside 2 in K value and it exhibited good clamping characteristics.

Fig. 5 shows the clamping voltage behavior for applied current impulse of 100 A/cm^2 with different Tb_4O_7 content. The varistors doped with 0.75 mol% and 1.0 mol% Tb_4O_7 were destroyed at the number of applied current impulse of 45 times and 22 times, respectively, and they lost the nonlinear properties. When Tb_4O_7 was added above 0.75 mol%, many

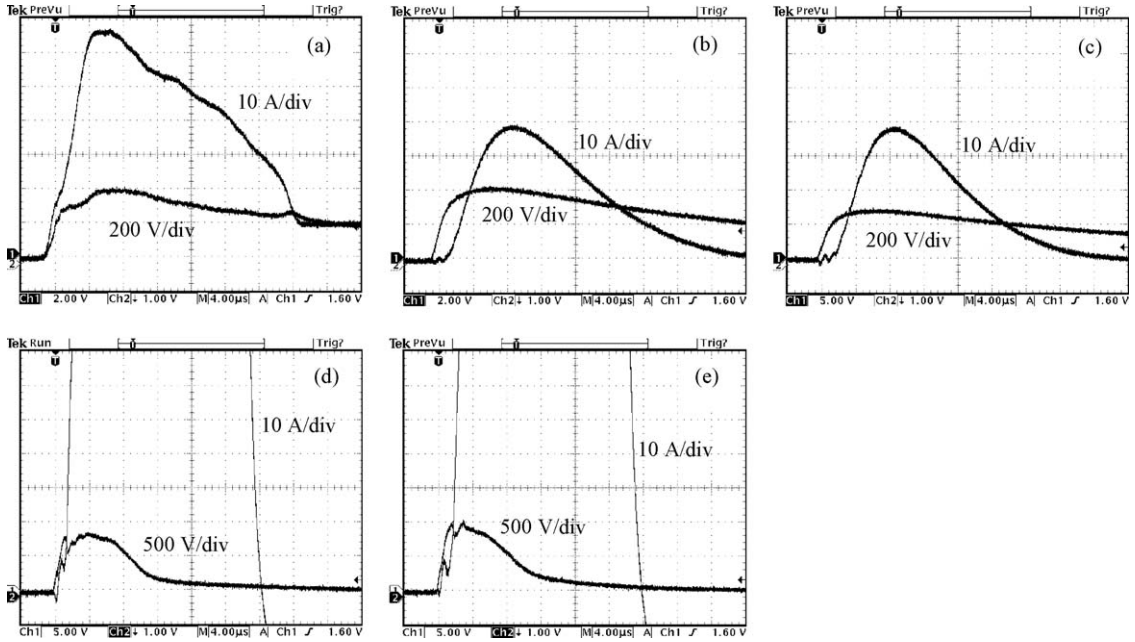

Fig. 5. Clamping voltage behavior during applying the current impulse of 100 A/cm^2 with different Tb_4O_7 contents: (a) 0.0 mol%, (b) 0.25 mol%, (c) 0.5 mol%, (d) 0.75 mol%, and (e) 1.0 mol%.

Table 2
Variations of breakdown field ($E_{1\,mA/cm^2}$), nonlinear coefficient (α), and current density (J_L) with the number of applied current impulse of 100 A/cm^2.

Tb_4O_7 content (mol%)	Number of applied current impulse (100 A/cm^2)	$E_{1\,mA/cm^2}$ (V/cm)	$\%\Delta E_{1\,mA/cm^2}$	α	$\%\Delta\alpha$	J_L (μA/cm^2)	$\%\Delta J_L$
0	Initial	1087		9.8		177.0	
	45	Failure					
0.25	Initial	1414	–	17.8	–	23.5	–
	100	1402	−0.8	18.3	2.8	21.9	−6.8
	400	1400	−1.0	17.8	0	20.9	−11.0
	700	1403	−0.8	18.0	1.1	18.9	−19.6
	1000	1402	−0.8	18.0	1.1	20.5	−12.8
0.5	Initial	3064	–	34.3	–	9.2	–
	100	3052	−0.4	34.0	−0.9	7.0	−23.9
	400	3038	−0.8	33.3	−2.9	6.5	−29.4
	700	3035	−0.9	33.3	−2.9	6.4	−30.4
	1000	3035	−0.9	33.2	−3.2	6.6	−28.3
0.75	Initial	5610		35.0		7.1	
	45	Failure					
1.0	Initial	6322		37.2		16.3	
	22	Failure					

Table 3
Variations of breakdown field ($E_{1\,mA/cm^2}$), nonlinear coefficient (α), and current density (J_L) with different current impulses.

Tb_4O_7 content (mol%)	Impulse current (A)	$E_{1\,mA/cm^2}$ (V/cm)	$\%\Delta E_{1\,mA/cm^2}$	α	$\%\Delta\alpha$	J_L (μA/cm^2)	$\%\Delta J_L$
0.25	Initial	1414	–	17.8	–	23.5	–
	500	1268	−10.3	15.7	−11.8	35.7	51.9
	900	6	−99.6	1.02	−94.3	655.2	2688
0.5	Initial	3064	–	34.3	–	9.2	–
	500	2696	−12.0	27.1	−21.0	2.2	−76.1
	900	2133	−30.4	17.9	−47.8	6.9	−25.0

secondary phases existed at grain boundary and triple point. This results in the decrease of effective area of the grain boundary. As a result, this failure against current impulse is attributed to very high current impulse density per grain boundary due to many secondary phases. In addition, the varistors doped with 0.75 mol% and 1.0 mol% Tb_4O_7 have a low electron concentration of ZnO grain [14]. A low donor concentration decreased the restriction effect for very high current impulse. This resulted in the destruction for the varistors. However, the varistors doped with 0.25 mol% and 0.5 mol% Tb_4O_7 exhibited very high stability against current impulse. This strongly suggests that Tb_4O_7 should be added less than 0.5 mol% in the ZPCC-based varistors. The *E–J* characteristic parameters after applying the current impulse are compared with initial *E–J* characteristics, as shown in Table 2. The $E_{1\,mA/cm^2}$ and α for the varistors doped with 0.25 mol% and 0.5 mol% Tb_4O_7 after applying the current impulse exhibited a low variation, within 3%. This also shows

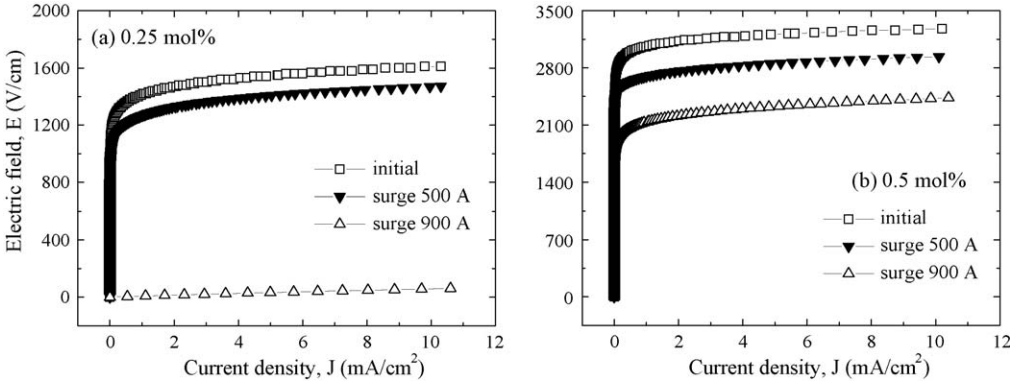

Fig. 6. *E–J* characteristics after applying the current impulses of 500 A and 900 A.

very high stable $E_{1\,mA/cm^2}$ and α characteristics: the $E_{1\,mA/cm^2}$ value decreased by 10–30 V/cm from the initial value after applying the current impulse and the α value decreased or increased by 1 from the initial value after applying the current impulse.

Fig. 6 shows *E–J* characteristics before and after applying the higher current impulses of 500 A and 900 A for the varistors doped with 0.25 mol% and 0.5 mol% Tb_4O_7. When a current impulse is 500 A, the varistor doped with 0.25 mol% Tb_4O_7 exhibited a smaller *E–J* characteristic variation than that of the varistor doped with 0.5 mol% Tb_4O_7. However, when a current impulse is 900 A, the varistor doped with 0.25 mol% Tb_4O_7 exhibited failure state, close to ohmic characteristics and contrasted with varistor doped with 0.5 mol% Tb_4O_7. Table 3 shows *E–J* characteristic variation after applying the current impulses of 500 A and 900 A for the varistors doped with 0.25 mol% and 0.5 mol% Tb_4O_7. The varistor doped with 0.5 mol% Tb_4O_7 exhibited a large variation by 30% in $E_{1\,mA/cm^2}$ and 50% in α, whereas they maintained the nonlinear properties with $\alpha = 18$.

4. Conclusion

The electrical behavior against current impulse in the Zn–Pr–Co–Cr-based varistors was investigated at different Tb_4O_7 contents. Tb_4O_7 did have a significant effect on electrical behavior against current impulse. Increasing Tb_4O_7 content improved clamp ratio (*K*), reaching nearly 2 at 1.0 mol%. The best stability against current impulse of 100 A/cm^2 was obtained at 0.25 mol% Tb_4O_7, where $\%\Delta E_{1\,mA/cm^2} = -0.8\%$ and $\%\Delta\alpha = +1.1\%$. On the other hand, the varistors doped with 0.5 mol% Tb_4O_7 exhibited the best surge withstand capability at a current impulse of 900 A. Conclusively, a moderate Tb_4O_7 content was optimized at 0.5 mol% in terms of the nonlinearity and surge withstand capability.

References

[1] L.M. Levinson, H.R. Philipp, Zinc oxide varistor—a review, Am. Ceram. Soc. Bull. 65 (1986) 639–646.

[2] T.K. Gupta, Application of zinc oxide varistor, J. Am. Ceram. Soc. 73 (1990) 1817–1840.

[3] C.-W. Nahm, The Electrical properties and d.c. degradation characteristics of Dy_2O_3 doped Pr_6O_{11}-based ZnO varistors, J. Eur. Ceram. Soc. 21 (2001) 545–553.

[4] A.B. Alles, V.L. Burdick, The effect of liquid-phase sintering on the properties of Pr_6O_{11}-based ZnO varistors, J. Appl. Phys. 70 (1991) 6883–6890.

[5] A.B. Alles, R. Puskas, G. Callahan, V.L. Burdick, Compositional effect on the liquid-phase sintering of praseodymium oxides-based ZnO varistors, J. Am. Ceram. Soc. 76 (1993) 2098–2102.

[6] Y.-S. Lee, K.-S. Liao, T.-Y. Tseng, Microstructure and crystal phases of praseodymium in zinc oxides varistor ceramics, J. Am. Ceram. Soc. 79 (1996) 2379–2384.

[7] C.-W. Nahm, The nonlinear properties and stability of ZnO–Pr_6O_{11}–CoO–Cr_2O_3–Er_2O_3 ceramic varistors, Mater. Lett. 47 (2001) 182–187.

[8] C.-W. Nahm, J.-S. Ryu, Influence of sintering temperature on varistor characteristics of ZPCCE-based ceramics, Mater. Lett. 53 (2002) 110–116.

[9] C.-W. Nahm, Microstructure and electrical properties of Y_2O_3 doped ZnO–Pr_6O_{11}-based varistor, Mater. Lett. 57 (2003) 1317–1321.

[10] C.-W. Nahm, B.-C. Shin, Highly stable electrical properties of ZnO–Pr_6O_{11}–CoO–Cr_2O_3–Y_2O_3-based varistor ceramics, Mater. Lett. 57 (2003) 1322–1326.

[11] C.-W. Nahm, Microstructure and electrical properties of Dy_2O_3-doped ZnO–Pr_6O_{11}-based varistor ceramics, Mater. Lett. 58 (2004) 2252–2255.

[12] C.-W. Nahm, B.-C. Shin, J. Mater. Sci.: Mater. Electron. 16 (2005) 725–732.

[13] C.-W. Nahm, Effect of sintering temperature on microstructure and electrical properties of Zn·Pr·Co·Cr·La oxide-based varistors, Mater. Lett. 60 (2006) 3394–3397.

[14] C.-W. Nahm, Electrical properties and aging characteristics of terbium-doped ZPCC-based varistors, Mater. Sci. Eng. B 137 (2007) 112–118.

[15] C.-W. Nahm, Microstructure and electrical properties of Al_2O_3-doped ZPCCYA-based varistors, Mater. Lett. 62 (2008) 2900–2903.

[16] J.C. Wurst, J.A. Nelson, Lineal intercept technique for measuring grain size in two-phase polycrystalline ceramics, J. Am. Ceram. Soc. 55 (1972) 109–111.